Chapter 4
On the Dynamic Virtualization of a 3D-Printed Scaled Wind Turbine Blade

Heorhi Brzhezinski, Silvia Vettori, Emilio Di Lorenzo, Bart Peeters, Eleni Chatzi, and Francesco Cosco

Abstract Innovative production techniques, such as 3D printing of metals, require attention both in the production and in the post-production phase. In fact, such manufacturing processes introduce higher margins of uncertainty compared to more canonical processes. As a consequence, they require an increased effort to succeed in delivering representations for the so-called dynamic virtualization process. Virtualization encompasses the ensemble of activities that are aimed at formulating the virtual model of a given structure and subsequently validating and updating this model in order to guarantee a realistic and accurate response prediction in a broad range of operating conditions. This chapter explores the main challenges related to the mentioned limitations, in the context of a down-scaled industrially relevant case study: a 3D-printed scaled titanium Wind Turbine (WT) blade. The scaled blade has been the object of a complete virtualization process: from the design by means of conventional WT blade tests, up to its "Digital-Twin" establishment, where we exploit state-of-the-art Virtual Sensing (VS) techniques, due to their intrinsic capability of "enriching" the high-fidelity model's predictions with information extracted from test data.

Keywords Wind turbine blades · 3D printing · Dynamic tests · Digital Twin · Virtual Sensing

4.1 Introduction

The 3D printing process of metals introduces technological challenges, e.g., limitations to 3D-printed specimens dimensions. For this reason, it is common practice to print the several sub-parts of the final product individually and then weld them together. Weld beads create areas of structural properties discontinuity that are difficult to be modeled. Moreover, intrinsic manufacturing process defects and thickness variations due to surface post-processing often arise. Canonical virtualization techniques produce realistic estimates under static conditions. Within the dynamic domain, the punctual stiffness variation caused by the mentioned limitations leads to large discrepancies between the "Digital Twin" and the physical structure. A model updating process based on experimental data can be installed to fill this gap. However, data acquired during dynamic tests derives from a few instrumented locations along the entire structure. The full-field response of the system can be obtained through the use of Virtual Sensing (VS) techniques [1–6], i.e., methods that allow to estimate quantities of interest by combining a limited set of measurements and a validated finite element (FE) model. Kalman-type filters are commonly adopted for the purpose of VS. When joint input-state-response estimation is addressed, extensions of the standard Kalman

H. Brzhezinski · F. Cosco
Department of Mechanical Engineering, Energy Engineering and Management, DIMEG, University of Calabria, Rende, Italy
e-mail: francesco.cosco@unical.it

S. Vettori (✉)
Siemens Digital Industries Software, Leuven, Belgium

Institute of Structural Engineering, ETH Zürich, Zürich, Switzerland
e-mail: silvia.vettori@siemens.com

E. Di Lorenzo · B. Peeters
Siemens Digital Industries Software, Leuven, Belgium
e-mail: emilio.dilorenzo@siemens.com; bart.peeters@siemens.com

E. Chatzi
Institute of Structural Engineering, ETH Zürich, Zürich, Switzerland
e-mail: chatzi@ibk.baug.ethz.ch

Z. Mao (eds.), *Model Validation and Uncertainty Quantification, Volume 3*, Conference Proceedings of the Society for Experimental Mechanics Series, https://doi.org/10.1007/978-3-031-04090-0_4

filter (KF) such as the Augmented Kalman filter (AKF) [7] and the Dual Kalman filter (DKF) [8] can be exploited. Within this work, the AKF [9] is tested on a 3D-printed scaled titanium Wind Turbine (WT) blade with the purpose of enriching its "Digital Twin" response predictions and performing load identification. The paper starts from Sect. 4.2, which describes the 3D-printed WT blade and the test campaign object of this work. The next section introduces the WT blade FE model and overviews the carried out model updating activities. Section 4.4 describes the results of the input-response estimation obtained via the AKF during the tests presented in Sect. 4.2.

4.2 3D-Printed Scaled Titanium WT Blade: Test Campaign

The case study analyzed in this chapter concerns a 3D-printed scaled titanium WT blade. The CAD model used to print the titanium blade has been retrieved scaling down an existing larger CAD model shared by DTU Wind Energy in the framework of the ReliaBlade research project. This CAD model is related to a 12.6m blade entirely designed and manufactured at DTU Wind Energy. The entire 3D-printed specimen, manufactured by 3D Systems (Leuven, Belgium), comprises the scaled blade and a flange that was designed to allow the blade clamping to a concrete block. Figure 4.1 shows the manufacturing process, which consisted of the following steps:

- Four sub-parts of the entire structure have been 3D-printed.
- A stress relief heat treatment has been applied to the four sub-parts.
- The four sub-parts have been welded together.
- The plate has been removed using wire through Electrical Discharge Machining (EDM).
- A polishing process has been applied to the structure to obtain the final surface.

This section describes the setup adopted during the test campaign carried out at Siemens Digital Industries Software (Leuven, Belgium) on the scaled blade, along with the series of tests performed with different types of excitation. Figure 4.2 shows the setup adopted during the measurements on the scaled WT blade. During all the hereby described tests, the WT blade was clamped to a concrete block as depicted in detail in Fig. 4.5.

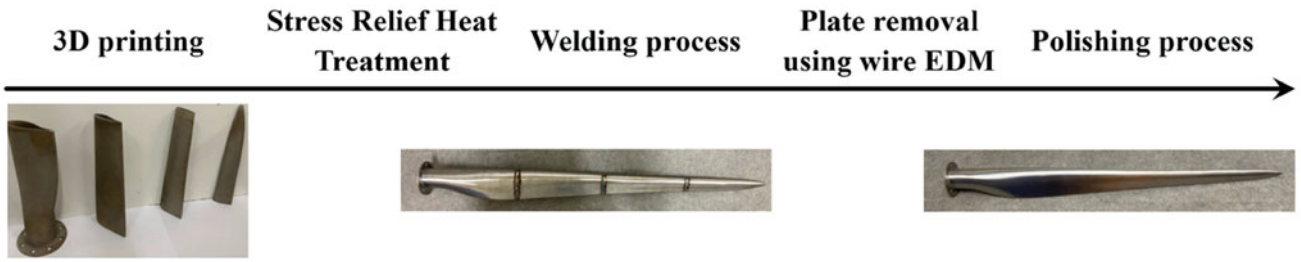

Fig. 4.1 3D-printed scaled titanium WT blade manufacturing process

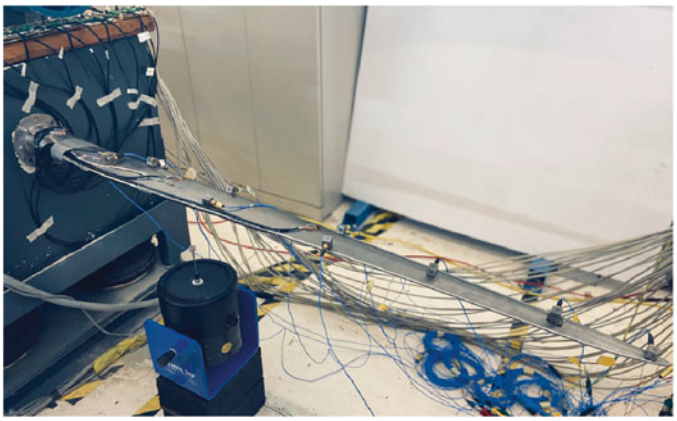

Fig. 4.2 Experimental setup

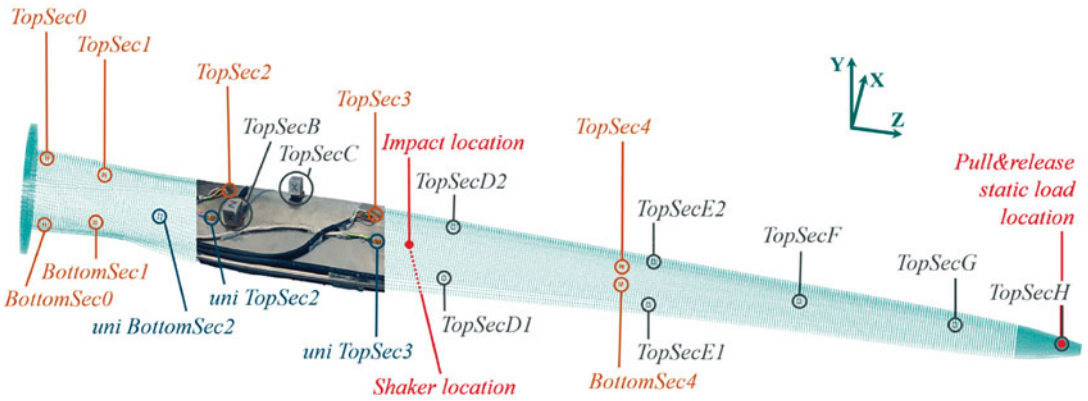

Fig. 4.3 Sensors' setup. USGs are reported in blue, rosettes in orange, accelerometers in black, and inputs locations in red

Table 4.1 Experimental modal frequencies and damping for the titanium WT blade in clamped-free conditions

Modes	Frequency (Hz)	Damping (%)
1	25.0	1.27
2	55.0	0.91
3	90.4	0.56
4	193.2	0.56
5	236.4	0.32
6	343.2	1.78

Fig. 4.4 Static load applied at the blade tip during pull and release tests

The entire setup includes 3 types of sensors: 4 uniaxial strain gauges (USGs), 10 rosettes, and 10 tri-axial accelerometers. During the test campaign, a Simcenter SCADAS system and Simcenter Testlab software have been used for data acquisition. The strain sensors are arranged in sections along the blade on both the top and bottom blade surfaces as shown in Fig. 4.3. On the other hand, the accelerometers have been positioned only on the top surface.

Three types of tests have been performed according to the adopted excitation: impact testing using a modal hammer, shaker testing, and the so-called pull and release tests. Figure 4.3 shows the locations of the impact and the shaker on the structure. Data acquired during the impact test has been used to determine the scaled WT blade modes, which have been extracted using Simcenter Polymax. Table 4.1 reports the resulting experimental frequencies and damping.

During shaker testing, constant frequency sine tests and continuous random tests up to 500 Hz were carried out. Finally, as common practice for WT blades, pull and release tests were carried out. During this type of tests, the blade in clamped-free boundary conditions (BCs) is pulled downward and then released for recording its free vibration response. As shown in Fig. 4.4, during the hereby described test campaign, the static load has been applied by hanging a mass (known weight equal to 1.5 kg) at the blade tip. The blade release has been reproduced by cutting the plastic tie used to hang the mass.

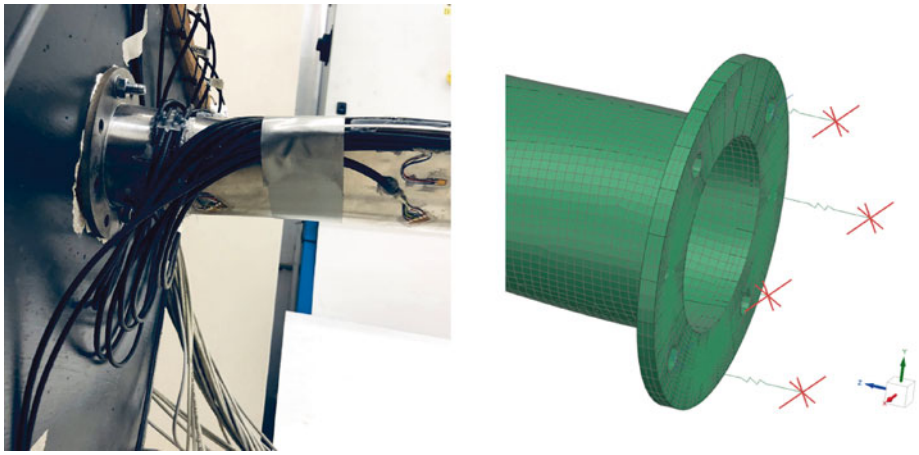

Fig. 4.5 Scaled WT blade clamping system (left). FE model BCs (right)

Table 4.2 FE model parameter values before and after optimization

	Spring's stiffness (N/mm)	Young's modulus (Gpa)	Poisson's ratio (/)	Density (kg/mm^3)
Initial values	30,000	121	0.34	4.430×10^{-6}
Final values	33,167.2	116.039	0.34208	4.873×10^{-6}

4.3 3D-Printed Scaled Titanium WT Blade: FE Model Validation

The scaled WT blade FE model has been developed in Simcenter 3D starting from the CAD model used for 3D printing. The mesh is made up of around 65,000 nodes and 33,804 six-sided solid elements. The initial isotropic material (Ti6Al4V) properties have been defined according to the data sheet provided by the manufacturer. Figure 4.5 (left) shows the physical BCs obtained by means of 2 bolts used to clamp the flange to the concrete block and a layer of glue. The described BCs have been recreated in the FE model through two RBE2 connections at the holes where the bolts were placed and four springs. In particular, the flange has been divided into four parts, each connected to a spring via a RBE2 connection. As shown in Fig. 4.5 (right), the free ends of the springs have been fixed. An initial stiffness value of 30,000 N/mm was used for each spring.

The numerical modes have been computed using NX Nastran SOL 103, and the frequency range 0–500 Hz has been chosen for validation. Experimental tests in this range have revealed the 6 natural frequencies reported in Table 4.1. In order to update the FE model, NX Nastran SOL 200 has been adopted in Simcenter 3D, and the experimental modes and frequencies reported in Sect. 4.2 have been used as reference. The following parameters have been set to be adjusted by the optimization: springs stiffness, isotropic material Young's modulus, Poisson's ratio, and density. Some of the ranges have been imposed from the processing data sheet provided by the manufacturer of the WT blade. The others were kept below a 10% deviation. Table 4.2 reports the parameters initial and optimized values.

Figure 4.6 shows the Modal Assurance Criterion (MAC) diagram between the reference experimental modes and the updated numerical modes. Table 4.3 reports the optimization results in terms of modal frequencies.

4.4 Joint Input-Response Estimation Through the AKF during Random and Pull and Release Tests on the 3D-Printed Scaled WT Blade

This work exploits the AKF for simultaneously estimating the 3D-printed WT blade response and the load it was subjected to during the shaker tests (continuous random excitation) and the pull and release tests described in Sect. 4.2. In order to reduce the computational effort derived by the high dimensionality of the FE model, a Reduced Order Model (ROM) has been built following the procedure described in [10–12]. The six normal modes reported in Fig. 4.6 have been used to build the ROM, along with one residual attachment mode related to the unknown (for the filter) force [11, 12]. The attachment mode has been computed as a static mode under a unitary input applied at the unknown excitation position. Therefore, two different attachment modes have been used for the pull and release and the continuous random tests.

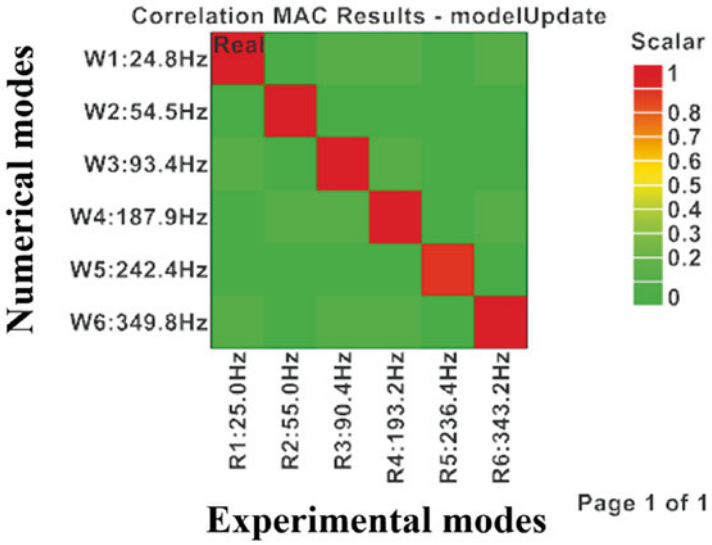

Fig. 4.6 MAC between numerical and experimental mode shapes from hammer test

Table 4.3 Experimental and updated numerical frequencies for the titanium WT blade in clamped-free conditions

Modes	Experimental frequency (Hz)	Numerical frequency (Hz)	Absolute error (Hz)	Percentage error (%)
1	25.020	24.758	−0.262	−1.047
2	55.004	54.512	−0.492	−0.894
3	90.426	93.405	2.979	3.294
4	193.201	187.902	−5.299	−2.743
5	236.416	242.358	5.942	2.513
6	343.176	349.807	6.631	1.932

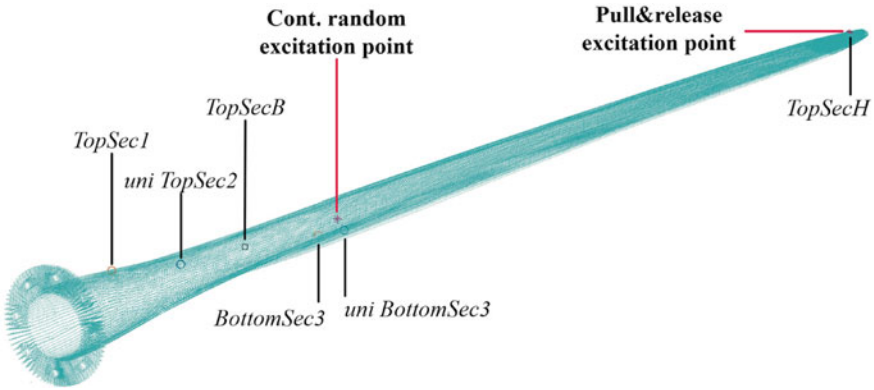

Fig. 4.7 Tests excitation points and "observed" locations for joint input-response estimation through the AKF

The AKF algorithm has been employed within this work to perform predictions basing on a set of measurements from different types of sensors, i.e., strain and acceleration. To check the effectiveness of the filter, only a few sensors over the entire set of responses acquired during tests were used as observations for the AKF. The remaining sensors data have been used as reference to check for the validity of the estimated responses. Figure 4.7 shows the observations set adopted for both the pull and release and the continuous random tests. In the framework of Kalman-type filters, model uncertainties and measurement errors are taken into account by including, respectively, the process and the measurement noise terms within the system representation. These are stationary mutually uncorrelated Gaussian noises with given associated covariance matrices. For the hereby presented case study, the measurement noise covariance has been retrieved from the background noise recorded by sensors during tests. The process noise covariance has been instead tuned by trial and error.

Figure 4.8 shows a comparison of the input time history estimated by the AKF (in magenta) and the actual input (in black) applied to the system for both the pull and release and the random tests. During the random tests, the force applied by the

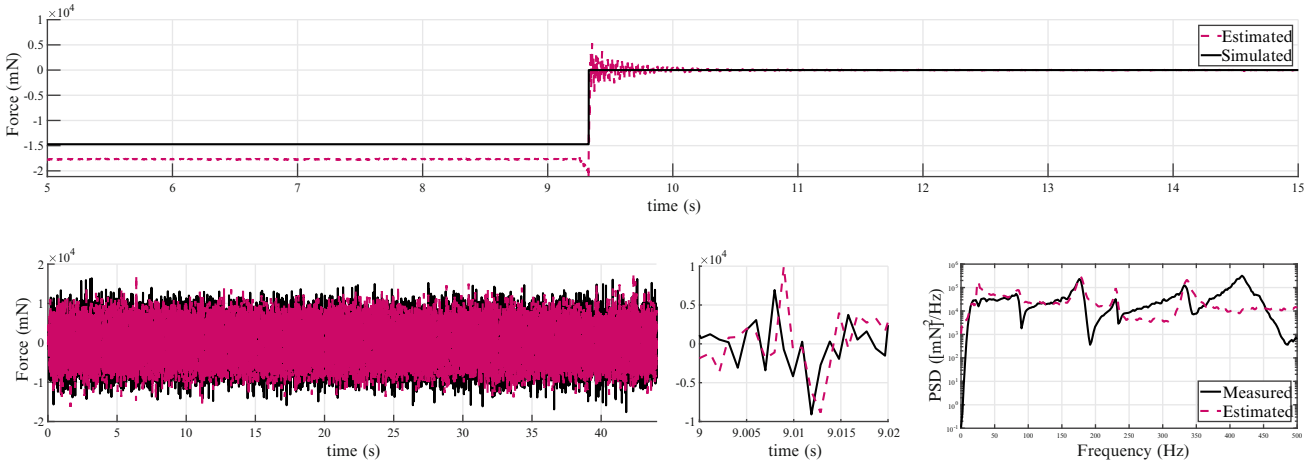

Fig. 4.8 Pull and release excitation history (top). Continuous random excitation time history (bottom, left), detailed time history (bottom, center), and PSD (bottom, right). Actual and predicted signals are, respectively, reported in black and magenta

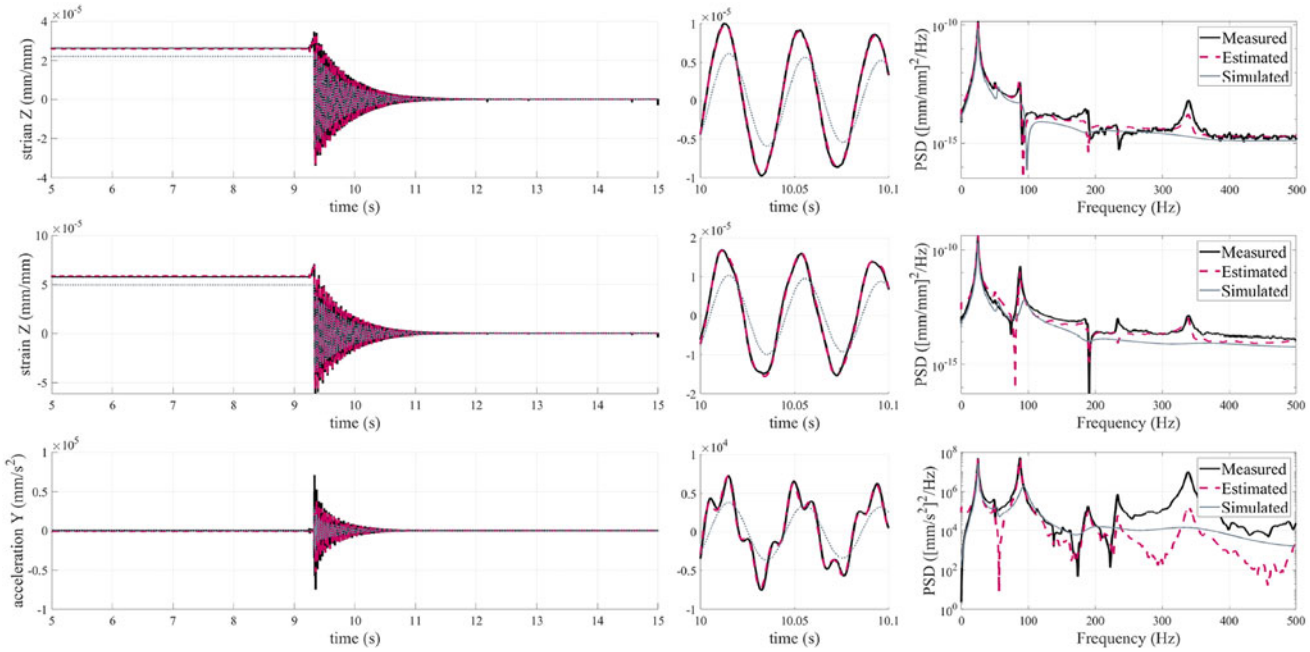

Fig. 4.9 Pull and release time histories (left), detailed time histories (middle), PSD (right) of sensors uni TopSec3, TopSec4, TopSecE2 (respectively, from top to bottom)

shaker has been recorded by a force cell placed between the shaker and the structure. During pull and release tests instead, the static input time history has been reconstructed from the known weight of the mass used to pull the blade. From Fig. 4.8, it can be inferred that the AKF is able to estimate the input during both tests.

For what concerns the pull and release test, an estimate of the prediction error can be computed as the difference between the actual static input and the mean value of the estimated input profile (before and after the blade release), which is equal to 1.32×10^3 mN. The static offset between the actual and the estimated input profiles before the blade release can be ascribed to the assumption of punctual loading made to approximate the input location in the model adopted for the AKF. For what concerns the continuous random test, the algorithm succeeds in estimating the correct input amplitude. On the other hand, the AKF generates an input featuring a flatter PSD with respect to the measured signal. The latter is highly affected by the blade resonances due to the specific BCs between the shaker and the structure. This behavior is difficult to be captured by the filter. The estimated input root mean square error (RMSE) is equal to 4.5126×10^3 mN.

Response estimation results are reported in Fig. 4.9 (pull and release) and in Fig. 4.10 (continuous random) for 3 "unmeasured" locations (a USG, a rosette, and an accelerometer). These plots compare the measured (black), simulated

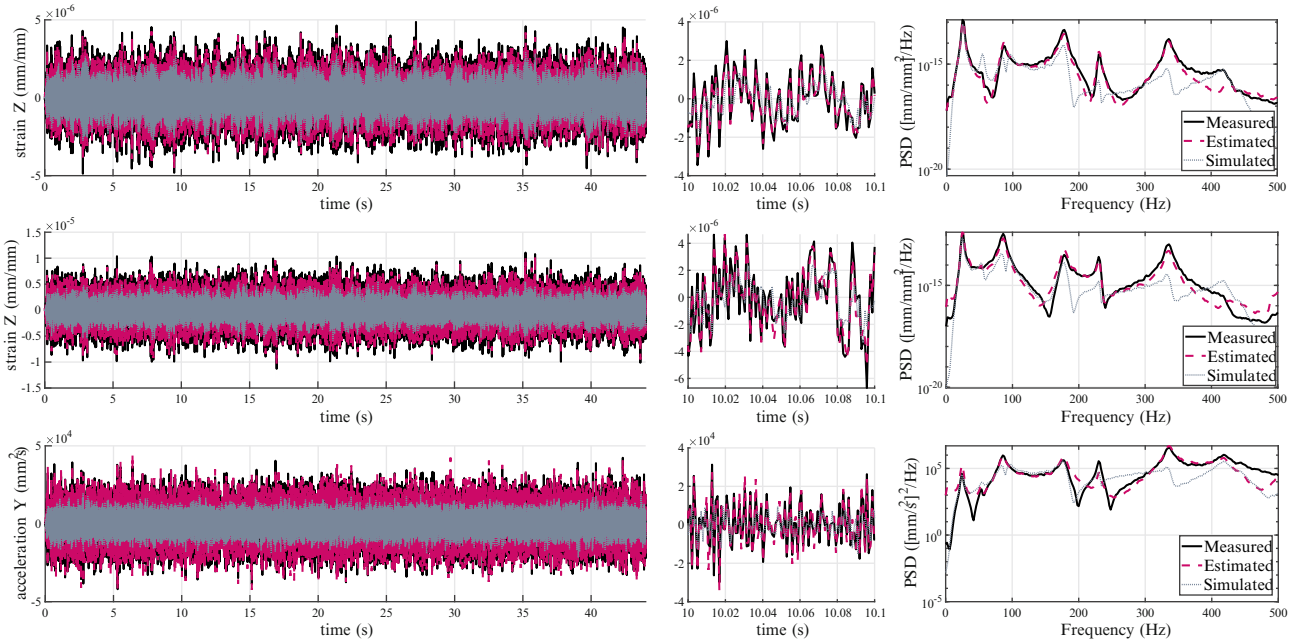

Fig. 4.10 Continuous random time histories (left), detailed time histories (middle), PSD (right) of sensors uni TopSec3, TopSec4, TopSecE2 (respectively, from top to bottom)

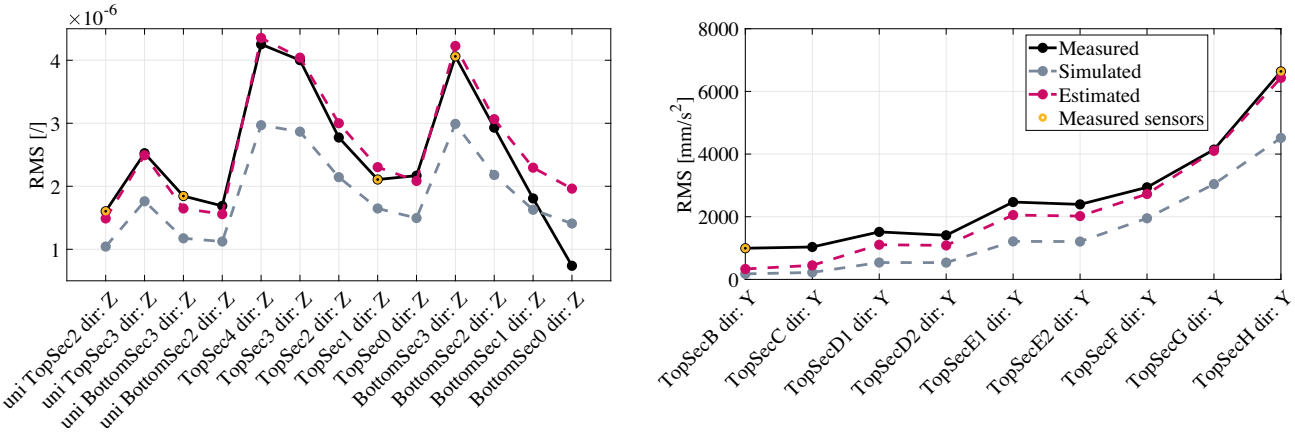

Fig. 4.11 Pull and release strain sensors RMS (left). Pull and release accelerometers RMS (right)

(gray), and estimated (magenta) signals in time and frequency domain. In order to demonstrate the filter performance, the root mean square (RMS) trend over the entire set of sensors along the blade is reported in Figs. 4.11 (pull and release) and 4.12 (continuous random) for the measured (black), simulated (gray), and estimated (magenta) responses. Figures 4.9, 4.10, 4.11, and 4.12 highlight the ability of the filter to correctly estimate the blade response, both in terms of strain and acceleration. Moreover, it is shown how the filter enhances the simulated responses by coupling the FE model with a few physical observations.

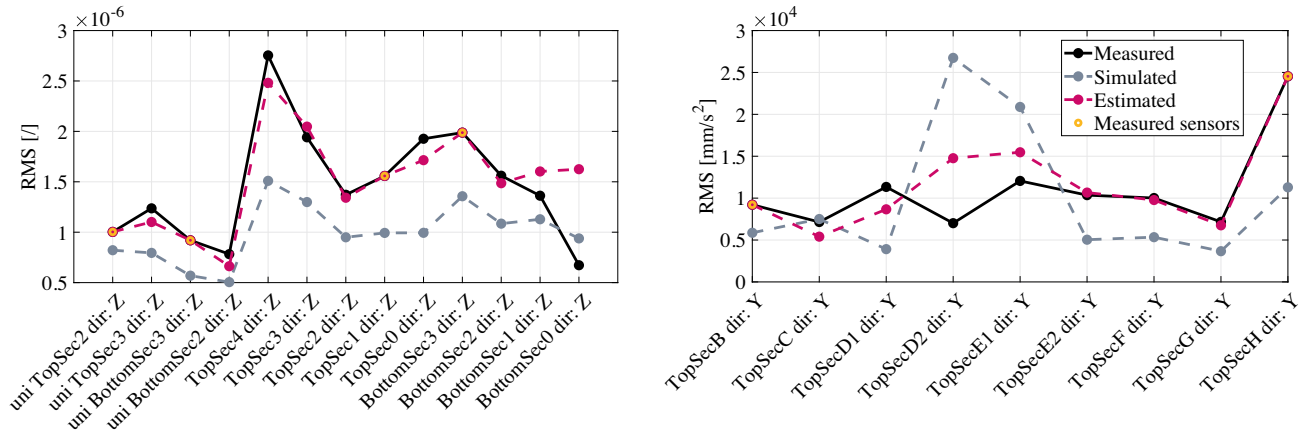

Fig. 4.12 Continuous random strain sensors RMS (left). Continuous random accelerometers RMS (right)

4.5 Conclusions

This chapter reports on the dynamic virtualization process installed for a 3D-printed scaled titanium WT blade. The individual steps of the process consisted in: (1) modeling the WT blade CAD model, (2) manufacturing the blade through an innovative 3D printing process, (3) building a FE model from the available CAD model, (4) testing the blade by means of conventional WT blades testing procedures, (5) validating and updating the FE model using experimentally extracted modal parameters, and (6) extending the information acquired during tests to the full-field response and simultaneously predicting the unknown loads by means of the AKF. This work has proven the effectiveness of the AKF results for both random and pull and release tests when a fusion of strain and acceleration responses is used. The next step could consist in applying other types of Bayesian filters that allow to jointly estimate the system state and parameters, along with the unknown loads. These tools could be used for estimating the defects due to the manufacturing process, e.g., the percentage of pores inside the artifact due to 3D printing.

Acknowledgments The authors gratefully acknowledge the European Commission for its support of the Marie Sklodowska Curie program through the ITN DyVirt project (GA 764547).

The authors would like to also acknowledge DTU Wind Energy and the project "RELIABLADE: Improving Blade Reliability through Application of Digital Twins over Entire Life Cycle," supported by the Danish Energy Agency through the Energy Technology Development and Demonstration Program (EUDP), Grant No. 64018-0068, the support of which is greatly appreciated.

References

1. Azam, S.E., Chatzi, E., Papadimitriou, C., Smyth, A.: Experimental validation of the Kalman-type filters for online and real-time state and input estimation. J. Vibration Control **23**(15), 2494–2519 (2017)
2. Dertimanis, V.K., Chatzi, E.N., Azam, S.E., Papadimitriou, C.: Input-state-parameter estimation of structural systems from limited output information. Mech. Syst. Signal Process. **126**, 711–746 (2019)
3. Papadimitriou, C., Fritzen, C.P., Kraemer, P., Ntotsios, E.: Fatigue predictions in entire body of metallic structures from a limited number of vibration sensors using Kalman filtering. Struct. Control Health Monit. **18**(5), 554–573 (2011)
4. Cumbo, R., Tamarozzi, T., Janssens, K., Desmet, W.: Kalman-based load identification and full-field estimation analysis on industrial test case. Mech. Syst. Signal Process. **117**, 771–785 (2019)
5. Vettori, S., DiLorenzo, E., Peeters, B., Chatzi, E.: Virtual sensing for wind turbine blade full field response estimation in operational modal analysis. In: Proceedings of IMAC2020 International Conference (2020)
6. Avitabile, P., Pingle, P.: Prediction of full field dynamic strain from limited sets of measured data. Shock Vibration **19**(5), 765–785 (2012)
7. Lourens, E., Reynders, E., De Roeck, G., Degrande, G., Lombaert, G.: An augmented Kalman filter for force identification in structural dynamics. Mech. Syst. Signal Process. **27**, 446–460 (2012)
8. Azam, S.E., Chatzi, E., Papadimitriou, C.: A dual Kalman filter approach for state estimation via output-only acceleration measurements. Mech. Syst. Signal Process. **60**, 866–886 (2015)
9. Maes, K.: Filtering techniques for force identification and response estimation in structural dynamics. PhD thesis, KU Leuven, 2016
10. Craig, R.J.: A review of time-domain and frequency-domain component mode synthesis methods. Int. J. Anal. Exp. Modal Anal. **2**(2), 59–72 (1987)

11. Vettori, S., Di Lorenzo, E., Peeters, B., Chatzi, E.: A virtual sensing approach to operational modal analysis of wind turbine blades. In: Proceedings of ISMA2020 International Conference on Noise and Vibration Engineering, Leuven, Belgium (2020)
12. Vettori, S., Lorenzo, E.D., Cumbo, R., Musella, U., Tamarozzi, T., Peeters, B., Chatzi, E.: Kalman-based virtual sensing for improvement of service response replication in environmental tests. In: Model Validation and Uncertainty Quantification, vol. 3, pp. 93–106. Springer (2020)